Diamond & Related Materials 82 (2018) 56–62

Contents lists available at ScienceDirect

Diamond & Related Materials

journal homepage: www.elsevier.com/locate/diamond

Hardness of diamond-cBN nanocomposite

Ruslana Balabai, Dariya Kravtsova*

Kryvyi Rih State Pedagogical University, 54 Gagarina Ave., Kryvyi Rih, 50086, Ukraine

ARTICLE INFO

Keywords:
Diamond-cBN nanocomposite
Hardness
The functional electron density
Ab initio pseudopotential

ABSTRACT

The spatial densities of valence electrons and their cross sections, the total energies, and the force response on the deformation for modeling objects of the cC-cBN composite were evaluated by methods of the electron density functional and *ab initio* pseudopotential.

The spatial distributions of the electron density of the chemical bonds C—B and C—N were obtained and discussed. The first principles calculation confirms that the chemical C—N bond stronger than the C—B bond; it affects the chemical inertness of different composite models.

In this computer experiment, the imaginary indenter penetration process is simulated as the gradual relocation of atoms deep into the cluster. When the model cubical crystal of the cC-cBN composite with as sequence of layers as C, N, and B was deformed at the top like on figure, the record high hardness and the low reactivity combined. Model crystals of the cC-cBN composite with other order of layers C, N, and B have the high value of hardness too, but electron density, squeezed to the surface of the cluster, casts doubt on the chemical stability.

In addition, it was identified physical mechanisms of the hardness of the materials, which have tetrahedral chemical bonds. The maps of the spatial distribution of the electron density of the deformed C—N bond illustrated the increasing concentration of electron density along this bond.

The changes of the total energy are interpreted as changes of the ionicity degree of deformed bonds in the model clusters.

1. Introduction

Diamond is used in the manufacture of the cutting tools often but it's the drawback is a high capacity to oxidation during the heating. In this regard, the search continues [1–5] some composites of the diamond with other solids that reduce chemical activity, but retain hardness. Today boron nitride is used for cutting steel industry due to its hardness and chemical stability. But its hardness is smaller (about 45 GPa) than hardness of diamond (about 115 GPa), therefore an increasing of the hardness of cBN remains the topical problem. In paper [6] shows that the nanotwinned c-BN is stronger than polycrystalline c-BN. But it is noted [7] that polycrystalline diamond and polycrystalline BN show higher mechanical strength than the monocrystalline samples, in addition, it is inversely proportional to the size of the grain. The research [8] reported that the additional coverage Ni/SiC on the surface of grains of cBN improves wear resistance significantly as a result the unique morphology of the growth of spikes Ni. Also known, that BN-nanotubes have the hardness and the tensile strength, which are close to diamond [9].

The composite of diamond and cubic boron nitride is the most probable potential candidate to the role of the universal cutting material. The excellent results showed the experimental samples in [10]. These composites consist of the sintered nanodiamonds and cBN with different ratios of diamond to boron nitride. The authors emphasize sample with a ratio of 2:1. The hardness reached 85 GPa, which measured a standard square-pyramidal indenter.

In [11] researchers created the prototype of the alloy diamond and cubic boron nitride (cC-cBN), which was 3 mm in diameter and was tested by the high cutting of the hardened steel and granite successful. Compared with commercial materials, the alloy cC-cBN showed the higher wear resistance, sufficient chemical inertness and hardness close to polycrystalline diamond.

The hardness called the property of the material to resist elastic and plastic deformation or destruction during indentation into it a more rigid body [12]. Mechanical hardness is defined as the ratio of the indentation load to the square of track in the sample.

This paper presents the results of the calculating experiment, which is performed using the software package [13]. It is clear that in a polyatomic system all other atomic cores and electronic subsystem act on any atom. One of the functions of the software [13] is a calculation

* Corresponding author.
E-mail address: gritsulia.dariya@kdpu.edu.ua (D. Kravtsova).

https://doi.org/10.1016/j.diamond.2017.12.016
Received 9 July 2017; Received in revised form 27 November 2017; Accepted 19 December 2017
Available online 21 December 2017

of such forces. Logical to assume that the force, which resists indentation load, is the difference between forces generated in undeformed and deformed material. Thus, the process of the indentation of the atomic model is possible to simulate. We relocate atoms in the model and recalculate the forces. In this way, the information about indentation load and depth of its track is obtained. Hardness is the quotient of division of the force, which applied to the model, to surface of the submerged sphere of indenter.

Used software is unique author's code, which has several advantages. Firstly, the authors take responsibility for any errors of algorithmic or mathematical nature in their own product. Second, the software has been tested in many scientific author's papers [14–18] successful. Third, the process of scientific physical analysis of calculation result is more flexible if you have your own open source; it is possible to analyze the results of any intermediate stage and see any data and not only those that are programmed by the third party developer. In addition, the improvement of software according to specific needs of the research independently is also convenient. Due to the fact that the software package is not yet registered, the [13] reference contains the application of control calculate of the spatial distribution of density and density of states of the valence electrons, the total energy of the silicon crystal.

2. Methods

The basic states of the electron-nuclear systems were detected by means of the self-consistent solution of the Kohn-Sham equations, because electronic variables only were determined with the atomic cores fixed. Following Kohn-Sham, electronic density was written down in terms of occupied orthonormal one-particle wavefunctions:

$$n(\mathbf{r}) = \sum_i |\psi_i(\mathbf{r})|^2 \tag{1}$$

The point on the surface of potential energy in the Born-Oppenheimer approximation was determined as a minimum energy functional with regard to the wavefunctions:

$$E[\{\psi_i\},\{R_j\},\{\alpha_\nu\}] = \sum_i \int_\Omega d^3r \psi_i^*(\mathbf{r})\left[-\frac{\hbar^2}{2m}\nabla^2\right]\psi_i(\mathbf{r}) + U[\{n(\mathbf{r})\},\{R_j\},\{\alpha_\nu\}], \tag{2}$$

where $\{R_j\}$ are coordinates of atomic cores; $\{\alpha_\nu\}$ are any external influences on the system.

In the generally accepted formulation, minimization of the energy functional (2) with respect to one-particle orbitals with additional orthonormal constraint on the one-particle orbitals $\psi_i(\mathbf{r})$ results in Kohn-Sham one-particle equations:

$$\left\{-\frac{\hbar^2}{2m}\nabla^2 + \frac{\partial U}{\partial n(\mathbf{r})}\right\}\psi_i(\mathbf{r}) = \varepsilon_i\psi_i(\mathbf{r}). \tag{3}$$

Distribution of electrons along the energy zones for Γ-state of catalyst structures was found by means of numerical calculation of derivative $\lim_{\Delta E\to 0} \Delta N/\Delta E$ (where ΔN is a number of the allowed states for the ΔE interval of energy). The one-particle energy spectrum was obtained from calculation of the eigenvalues of the Kohn-Sham matrix. In accordance with ideology of the electronic density functional, the occupied states at absolute zero temperature were defined. It allowed to define position of the last occupied state, their number being half the number of electrons (due to ignoring the spin of the electron), and position of the first free states.

We use the Bachelet-Hamann-Schlüter pseudopotentials [19,20] for calculating the potentials of interactions in the solution of the Kohn-Sham equations. Calculation implements in part of the author's software [13].

The total energy on a unit cell has the form:

$$E_{tot}/\Omega = \sum_{\mathbf{k},\mathbf{G},i} |\Psi_i(\mathbf{k}+\mathbf{G})|^2 \frac{\hbar^2}{2m}(\mathbf{k}+\mathbf{G})^2 + \frac{1}{2}4\pi e^2 \sum_{\mathbf{G}}{}' \frac{|\rho(\mathbf{G})|^2}{\mathbf{G}^2} + \sum_{\mathbf{G}} \varepsilon_{xc}(\mathbf{G})\rho^*(\mathbf{G}) + + \sum_{k,\mathbf{G},\mathbf{G}',i,l,s} S_s(\mathbf{G}-\mathbf{G}')\Delta V_{l,s}^{NL}(\mathbf{k}+\mathbf{G},\mathbf{k}+\mathbf{G}')\Psi_i(\mathbf{k}+\mathbf{G})\Psi_i^*(\mathbf{k}+\mathbf{G}') + + \sum_{\mathbf{G},s}{}' S_s(\mathbf{G})V_s^L(\mathbf{G})\rho^*(\mathbf{G}) + \left\{\sum_s \alpha_s\right\}\left[\Omega^{-1}\sum_s Z_s\right] + \Omega^{-1}\gamma_{Ewald}. \tag{4}$$

where $\mathbf{k}$ is the value from the first Brillouin zone, $\mathbf{G}$ – vector of the reciprocal lattice, $\Psi_i(\mathbf{k}+\mathbf{G})$ – the single-particle electron wave function, i – denotes the occupied states for a specific $\mathbf{k}$, $\rho(\mathbf{G})$ is coefficient in expanding the valence electron density, Σ' – primes in the summation exclude $\mathbf{G} = 0$ term, $\boldsymbol{\tau}$- the number of atoms in the unit cell, $S_s(\mathbf{G})$ is a structural factor, V_s^L is the local (l-independent) spherically symmetric pseudopotential, 1 denotes the orbital quantum number, $\Delta V_{l,\ \boldsymbol{\tau}}^{NL}$ is a nonlocal (1-dependent) additive V_s^L, Z_s – charge of an ion, γ_{Ewald} is the energy of Madelung of the point ions in a uniform negative background.

The force acting on atom s is the negative derivative of E_{tot} with respect to a basis vector $\boldsymbol{\tau}_s$. The terms containing implicit derivatives of the wave functions vanish according to Hellmann-Feynman theorem. Therefore, the calculation of forces is performed by a simple formula:

$$\mathbf{F}^s = \mathbf{F}_e^s + \mathbf{F}_c^s, \tag{5}$$

where components of electronic and ionic interactions are defined:

$$\mathbf{F}_e^s = i\Omega_c \sum_{\mathbf{G}} \rho^*(\mathbf{G})\mathbf{G}e^{-i\mathbf{G}\boldsymbol{\tau}_s}\upsilon_s(\mathbf{G}) - \sum_{i,\mathbf{G},\mathbf{G}',l} n_i\Psi_i^*(\mathbf{k}_i+\mathbf{G}')\Psi_i(\mathbf{k}_i+\mathbf{G})(\mathbf{G}-\mathbf{G}')e^{-i(\mathbf{G}-\mathbf{G}')\boldsymbol{\tau}_s}\upsilon'_{s,l}(\mathbf{k}_i+\mathbf{G},\mathbf{k}_i+\mathbf{G}'), \tag{6}$$

$$\mathbf{F}_c^s = 2Z_s \sum_{s'\neq s} Z_{s'}\frac{4\pi}{\Omega_c}\sum_{\mathbf{G}}{}'\left(\frac{\mathbf{G}}{|\mathbf{G}|^2}\sin(\mathbf{G}(\mathbf{T}_s-\boldsymbol{\tau}_{s'}))e^{-\frac{|\mathbf{G}|^2}{4\eta^2}}\right) + 2Z_s\sum_{s'\neq s} Z_{s'}\sum_{\mathbf{l}}\left(\frac{\mathbf{x}\,\mathrm{erfc}(\eta\ |\mathbf{x}|)}{|\mathbf{x}|^3} + \frac{2\eta\mathbf{x}}{\sqrt{\pi}\ |\mathbf{x}|^2}e^{-|\mathbf{x}|^2}\right). \tag{7}$$

There are $\mathbf{x} = \mathbf{l} + \boldsymbol{\tau}_s - \boldsymbol{\tau}_{s'}$, Ω_c – cell volume per atom, $\boldsymbol{\tau}_s$ – basic vector of atom s, Z_s – core's charge, l – lattice vector, η – parameter of the convergence of the amount in the Ewald's function erfc.

To calculate the exchange and correlation energies we used Ceperley-Alder's approximation that has been parameterized by Perdew and Zunger. Integration by k was replaced by calculation at Γ-point. Attention should be paid to the fact that the Γ-point for superlattice calculations has the value of the Baldereschi mean-value point, which represents all vectors in the Brillouin zone.

As the calculation algorithm envisages translational symmetry in the explored atomic system, initially, the orthorhombic type artificial superlattice was created. The research object determined parameters of the superlattice and the atomic base. For simulation of the cluster structure, the lattice parameters along Z, X, Y-axes was chosen so that the translationally located clusters would not influence one another.

3. Results and discussion

To separate the mechanical properties and the electronic characteristics of the model objects of the cC-cBN composite and the similar characteristics of the pure diamond and boron nitride, the model objects by such chemical compositions were developed. Comparative analysis is adequate because the calculation of the diamond objects, the objects of boron nitride and their composites is performed using only the same theoretical approach.

The model objects of the first group are the infinite films in the plane XY. The thickness of diamond and composite films are 5 Å, but

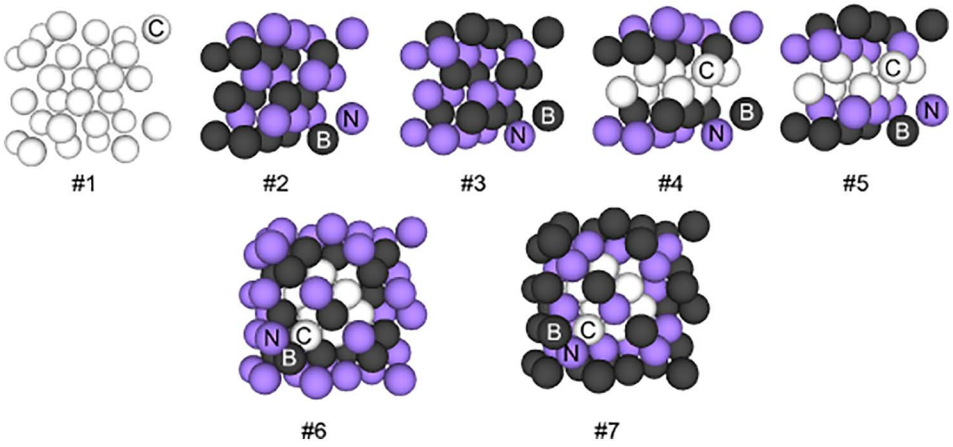

Fig. 1. Model nanocrystals of diamond (#1), boron nitride (#2, #3) and cC-cBN composite (#4–7).

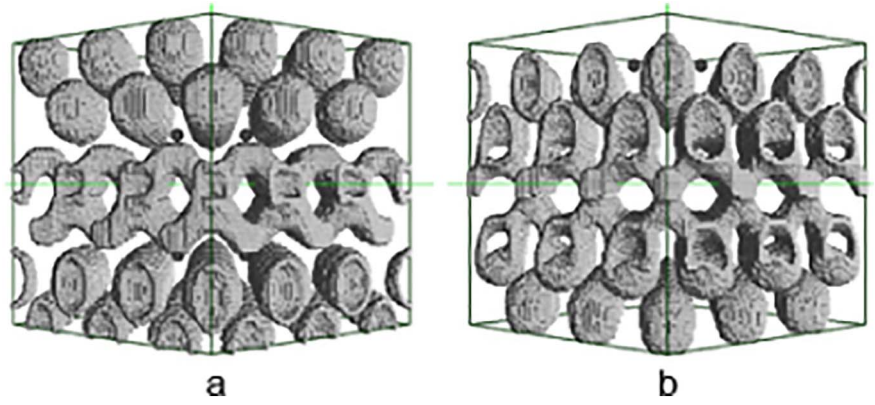

Fig. 2. The spatial distributions of the valence electron density in the film composite cC-cBN within the interval of 0.2–0.1 of the maximum value (boron to diamond - a, nitrogen to diamond - b).

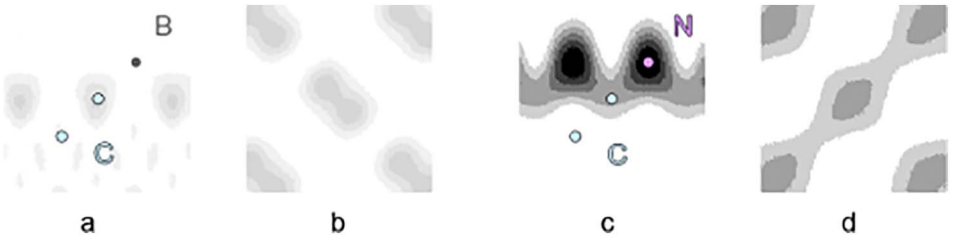

Fig. 3. The cross sections [110] (a, b) and [100] (c, d) of valence electron density in the area of the transition from the diamond to BN in the film composite cC-cBN (boron to diamond - a, b; nitrogen to diamond - c, d).

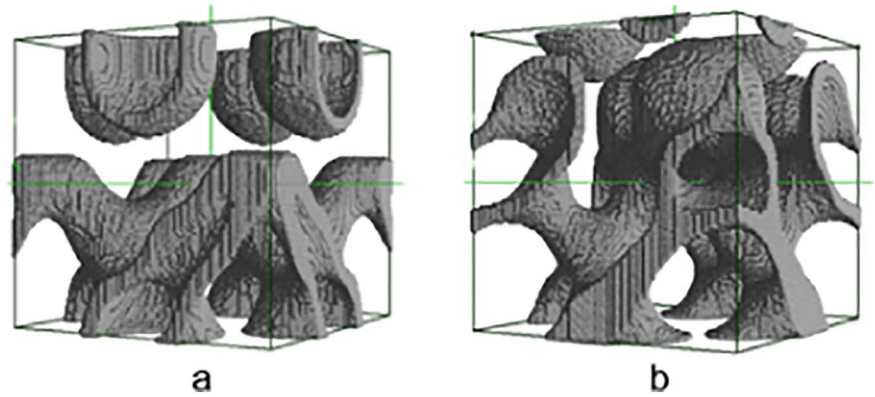

Fig. 4. The spatial distributions of the valence electron density in the area of the transition from the diamond to BN in the film composite cC-cBN within the interval of 0.2–0.1 of the maximum value (boron to diamond - a, nitrogen to diamond - b).

BN-films are 5,37 Å. Films of the cC-cBN composite are consisted of two layers of diamond, which were covered by a monolayer of boron initially and then by a monolayer of nitrogen or *vice versa*. The cBN films were compressed in 0.0056 times for all composite objects in our calculation (a(C) = 3,57 Å, a(BN) = 3,59 Å). The ratio of the number of diamond atoms to the number of atoms of boron nitride is 1:2 on per unit of volume of the composite.

The model objects of the second group are the nanocrystals (Fig. 1). The #1 object is the clean diamond crystals, the #4 object and #5 are the nanocrystals of diamond, which were covered by cBN on both sides; the dimensions of clusters are 5 Å. The ratio of the number of diamond atoms to the number of atoms of boron nitride is 2:5 in the #4 cluster

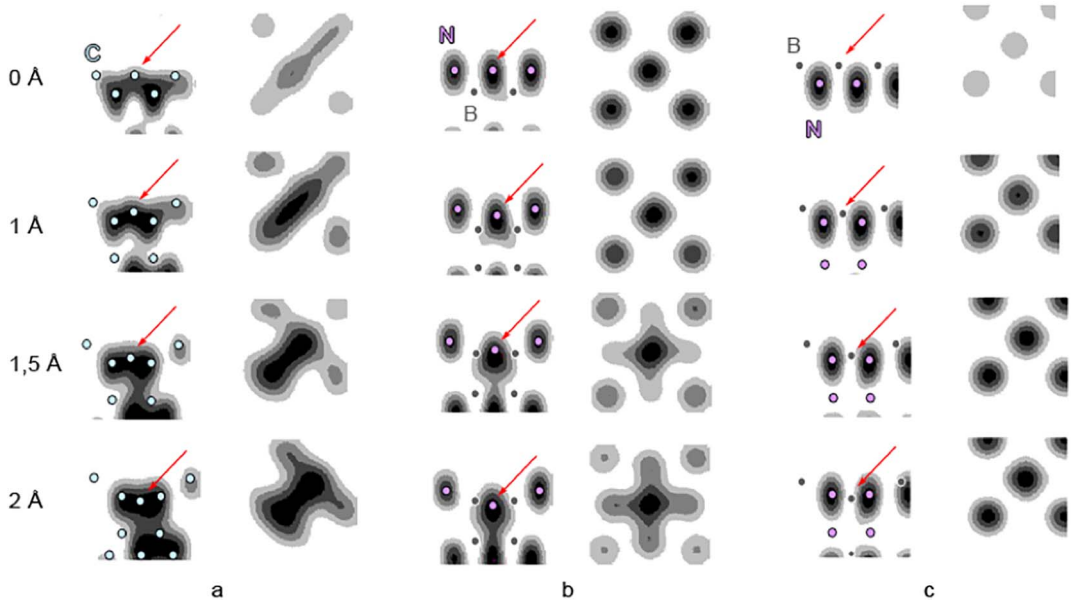

Fig. 5. The cross sections [110] and [100] of valence electron density of the model clusters #1 (a), #2 (b), #3 (c) during indentation on the surface. Moving atom is marked by the arrow.

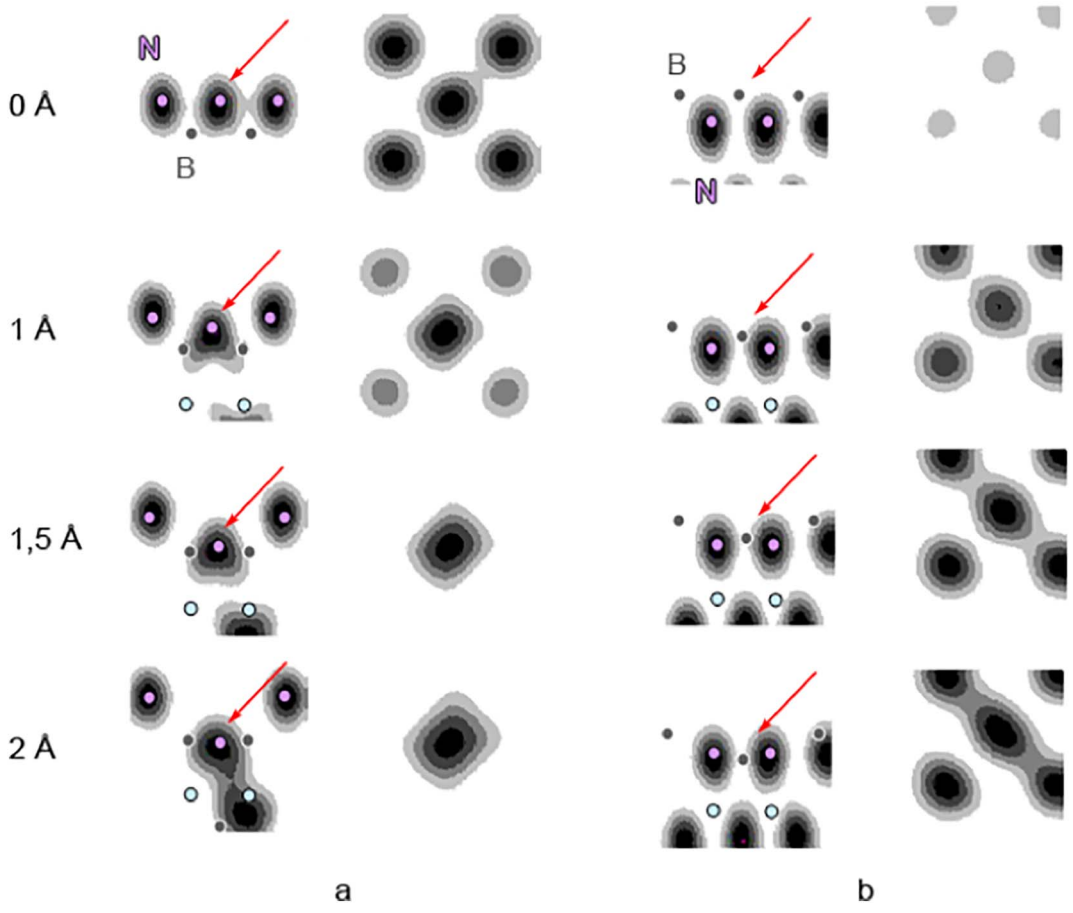

Fig. 6. The cross sections [110] and [100] of valence electron density of the model clusters #4 (a), #5 (b), during indentation on the surface. Moving atom is marked by the arrow.

and #5. The #2 cluster and the #3 cluster are crystals of clean cBN with size of 5,37 Å. The #6 and #7 models have a size of 7,12 Å and they are nanocrystals of diamond that covered by cBN on all sides. Here the number of atoms of diamond to the number of atoms of boron nitride is divided as 1:7.

The atomic bases of the film objects contained 48 atoms, clusters #1–5 contained 28 atoms, clusters #6–7 contained 64 atoms.

The form of the indenter, which is put into the model clusters, is ball of radius of 2,5 Å. The process of penetration is simulated by creating of defect that repeats form of the spherical indenter on the surface of the film or on the surface and in the top of the model nanocrystals.

The calculated data were in non-self-consistent version. The

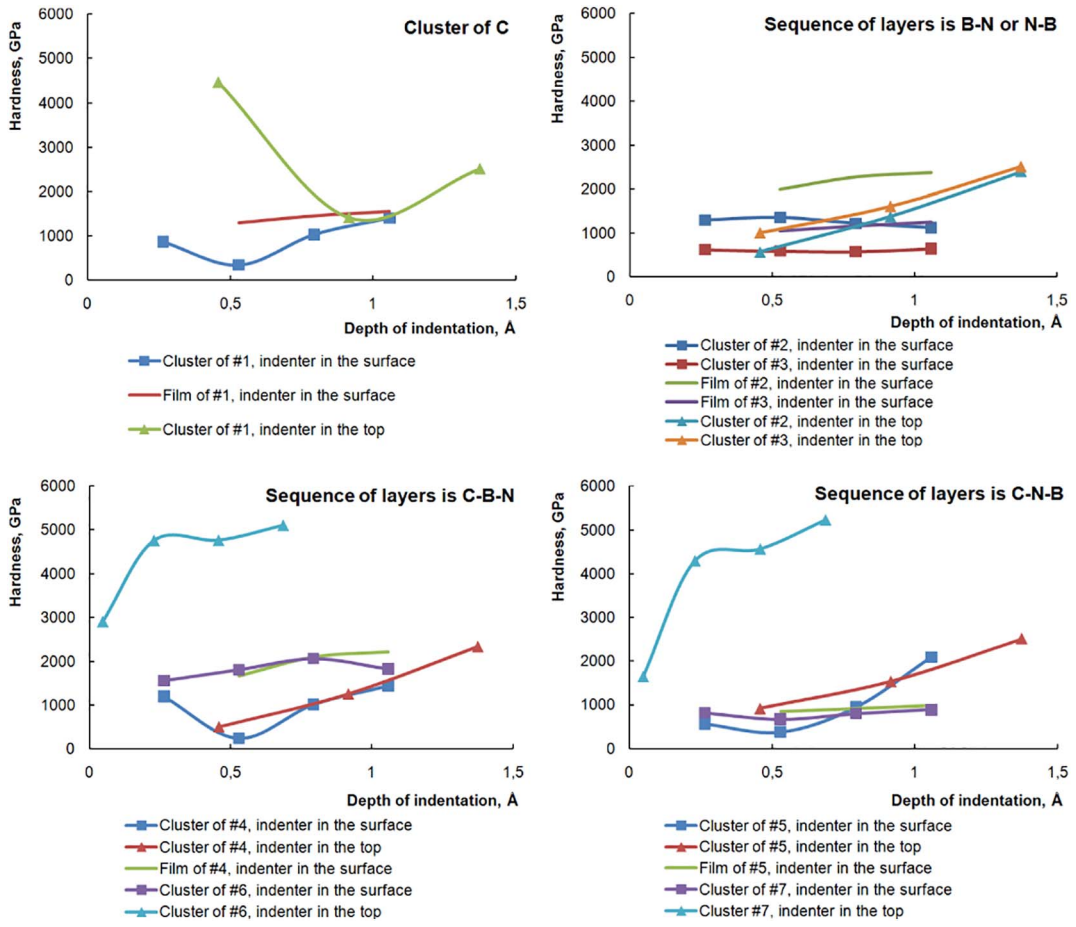

Fig. 7. Dependence of hardness during the indentation. Triangular markers illustrate the indentation in cluster's top, square – in the surface, without the marker – in the surface of the film models.

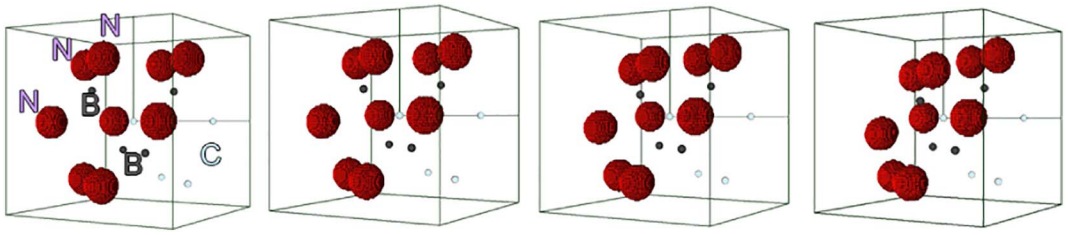

Fig. 8. The fragments of the spatial distribution of valence electron density in the orientational defect area for model #6 within the interval of 0.7–0.8 of the maximum value (indentation depth from 0,265 to 1058 Å left to right).

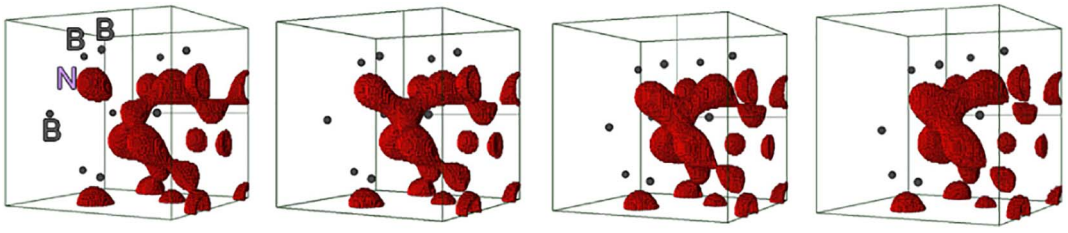

Fig. 9. The fragments of the spatial distribution of valence electron density in the orientational defect area for model #7 within the interval of 0.7–0.8 of the maximum value (indentation depth from 0,265 to 1058 Å left to right).

parameters of crystals were taken from the handbook [21]. To remove from the analysis of the forces that arise in developed unrelaxed atomic models, we analyzed the difference of forces arising between the ideal cluster and the defective cluster.

It was showed the spatial distribution of the valence electrons of the composite models of cC-cBN on Figs. 2 to 3. It is known that nitrogen is second only to F and O (sometimes Cl) in electronegativity, then carbon and boron have more ability to give electrons. On Figs. 2 to 3 the valence electrons are concentrated near the core of nitrogen mainly that corresponds to what has been said above.

In research [11] it was found that the binding energy of C—N atoms significantly exceeds the energy of C—B atoms in the cC-cBN composite

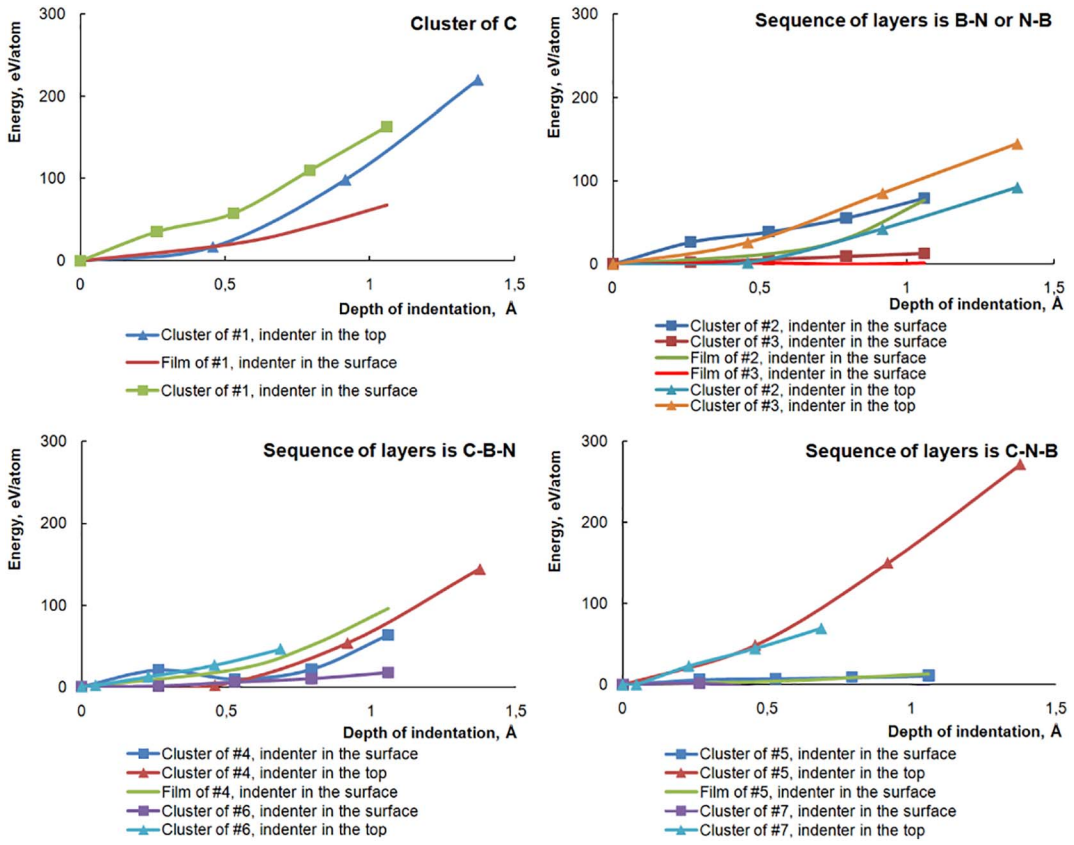

Fig. 10. The total energy of atomic systems during the indentation.

by the method of X-ray photoelectron spectroscopy. Indeed, the results of our calculations, which presented in Figs. 2 to 4, are showed that the C—N chemical bonds are stronger than the C—B bonds. Therefore, there is reason to believe that the composite objects with the boron's surface layer or the nitrogen's surface layer will show the differences in their physical characteristics.

Figs. 5 to 6 demonstrate that the electron density concentrated along the tetrahedral bond, when the spatial defect was creating by a virtual indenter. In other words the chemical bonds are strained; the bond lengths and angles between adjacent bonds are changed. This type of defect was described in [22]. It is alleged if an ideal structure of the lattice disturbed, the majority of bonds that were in undefect crystal kept, but they are modified. This is called the orientation defect. It manifests itself in varying degrees depending on the type of bonds between atoms in the crystal, and it influences the macroscopic physical properties of the object. Indeed, when comparing the cross section of the electron density of clusters with numbers of #1 to #5 you can see that the strained bonds are not so strong in the #3 object and #5 whose surfaces are covered with boron as compared with objects of #1, #2 and #4.

The curves of hardness on the depth of immersion of indenter are showed in Fig. 7. The hardness increases with the deepening, which is consistent with the experimental research microhardness of molybdenum in [12]. We consider that the calculation of the model objects hardness proved to 10 times higher compared to the experimental values, so that the hardness of nanoobjects are enhanced by their small surface area.

The graphics of the object's hardness, which are shown in Figs. 5 to 6, illustrate that the increased concentration of the electron density along the bond creates considerable resistance to deformation. So cluster of #3, which manifests little “strained” bonds, has the lowest value of the hardness (see Fig. 7(b)) compared to other objects with similar indentation.

The best performances of the hardness in each group of models have objects covered with nitrogen or boron. However, the high electronegativity of nitrogen is a risk that it will react with the surface of indenter or with the environment, which leads to a drastic reduction in range of applications of the nitrogen coverage. The lower hardness values are obtained for the models covered by boron, but reasons are to think that such composites are a chemically inert.

When crystal of the cC-cBN composite with as sequence of layers as C, N and B was deformed at the top, then the record high hardness and the low reactivity combined. Fig. 8 shows the spatial distribution of the density of valence electrons for the model cluster of #6 and Fig. 9 shows for #7. They illustrate that the electron density is concentrated within the cluster #7 mainly. During indentation of the nitrogen atom, which was at the top this cluster, the orientation defect is formed. In other words the chemical bond N—C is strained unlike B—C in Fig. 8. The figure shows that the defect is not manifested at this value of the electron density.

Graphs of total energy steadily increase in the most model calculations except energy of BN-objects covered with nitrogen, as shown in Fig. 10. On graphs 10 (b) and (c) it can be observed the extreme points for cluster of #2 and #4 at indentation to the surface. We think that they were due to increase of ionic interaction between atoms N, which indented, and neighboring B by decreasing the distance between them. It is known [23] that the degree of ionicity not exceed 20–25% of the crystal BN, and it means that a quarter of interactions are Coulomb nature in cluster. On the first displacement step on graphs only one atom of cluster offset on 0.5 b.r., so changing ion interaction was stronger than covalent. With increasing deformation four neighboring atoms are displaced, but not close to each other. This is followed by small changing of Coulomb interaction, and significantly increasing of covalent interaction, so energy continued to grow monotonically.

4. Conclusions

The spatial densities of valence electrons and their cross sections, the total energies and hardness as a function of the mechanical load for modeling objects of cC-cBN composite were evaluated by methods of the electron density functional and *ab initio* pseudopotential.

The best performances of the hardness are obtained for objects covered with nitrogen or boron. However, the high electronegativity of nitrogen is a risk that it will react with the surface of indenter or with the environment. When crystal of the cC-cBN composite with as sequence of layers as C, N and B was deformed at the top, then the record high hardness and the low reactivity combined. So, cC-cBN composite is a successful material for the manufacture of cutting tools or protective surfaces.

It was identified physical mechanisms that define hardness of the materials, which have tetrahedral chemical bonds. It was observed that when the defect that indenter creates, appears, than the electron density concentrates along the tetrahedral bonds.

References

[1] R.B. Kaner, J.J. Gilman, S.H. Tolbert, Designing superhard materials, Science 308 (2005) 1268–1269 5726.
[2] P.F. McMillan, New materials from high-pressure experiments, Nat. Mater. 1 (1) (2002) 19–25.
[3] A.R. Badzian, Cubic boron nitride-diamond mixed crystals, Mater. Res. Bull. 16 (11) (1981) 1385–1393.
[4] S. Koizumi, T. Murakami, T. Inuzuka, K. Suzuki, Epitaxial growth of diamond thin films on cubic boron nitride {111} surfaces by dc plasma chemical vapor deposition, Appl. Phys. Lett. 57 (6) (1990) 563–565.
[5] X.W. Zhang, H.G. Boyen, N. Deyneka, P. Ziemann, F. Banhart, M. Schreck, Epitaxy of cubic boron nitride on (001)-oriented diamond, Nat. Mater. 2 (5) (2003) 312–315.
[6] Y. Tian, B. Xu, D. Yu, Y. Ma, Y. Wang, Y. Jiang, Z. Zhao, Ultrahard nanotwinned cubic boron nitride, Nature 493 (7432) (2013) 385–388.
[7] H. Sumiya, K. Harano, Innovative ultra-hard materials: Binderless Nano-polycrystalline diamond and Nano-polycrystalline cubic boron nitride, Sci. Tech. Rev. 82 (2016) 21.
[8] Y. Gui, J. Zhao, J. Chen, Y. Jiang, Preparation and characterization of Ni spines grown on the surface of cubic boron nitride grains by electroplating method, Mater. Des. 9 (3) (2016) 153.
[9] X. Chen, L. Zhang, C. Park, C.C. Fay, X. Wang, C. Ke, Mechanical strength of boron nitride nanotube-polymer interfaces, Appl. Phys. Lett. 107 (25) (2015) 253105.
[10] X. Liu, X. Chen, H.A. Ma, X. Jia, J. Wu, T. Yu, S.D. Jacobsen, Ultrahard stitching of nanotwinned diamond and cubic boron nitride in C2-BN composite, Sci. Rep. 6 (2016) 30518.
[11] P. Wang, D. He, L. Wang, Z. Kou, Y. Li, L. Xiong, J. Liu, Diamond-cBN alloy: a universal cutting material, Appl. Phys. Lett. 107 (10) (2015) 101901.
[12] A.G. Kolmakov, V.F. Terentev, M.B. Bakirov, Methods of Measuring Hardness, Intermet Inzhuniring, Moscow, 2005.
[13] Ab initio calculation, http://sites.google.com/a/kdpu.edu.ua/calculationphysics (2015).
[14] R.M. Balabai, Electronic properties of functionalized graphene nanoribbons, Ukr, J. Phys. 58 (4) (2013) 389–397.
[15] R.M. Balabai, H.N. Chernikova, Platinum–nickel alloy catalysts for fuel elements, Appl. Phys. A Mater. Sci. Process. 116 (2) (2014) 649–655.
[16] R.M. Balabai, et al., Electron structure and dielectric matrix of the model photonic crystals formed by fibers: ab initio calculation, Nanosyst. Nanomater. Nanotechnol. 13 (4) (2015) 707–720.
[17] R.M. Balabai, D.Yu. Gritsulia, V.G. Litovchenko, Tuning of electron states of transition Metal's catalysts using Acceptor's atoms: ab initio calculation, J. Nano Electron. Phys. 8 (2) (2016) 02007.
[18] R.M. Balabai, A.V. Zdeschyts, A.G. Lubenets, Spectral and barrier properties of heterocomposites based on poly (para-phenylene) disposed between the silicon films, Mol. Cryst. Liq. Cryst. 639 (1) (2016) 39–46.
[19] D.R. Hamann, M. Schlüter, C. Chiang, Norm-conserving pseudopotentials, Phys. Rev. Lett. 43 (20) (1979) 1494.
[20] G.B. Bachelet, D.R. Hamann, M. Schlüter, Pseudopotentials that work: from H to Pu, Phys. Rev. B 26 (8) (1982) 4199.
[21] A.L. Ivanovskyi, G.P. Shveykin, Quantum Chemistry in Materials Science. Non-metallic Refractory Compounds and Non-Metallic Ceramics, Ekaterinburg, Ekaterinburg, (2000).
[22] V.S. Vavilov, A.E. Kiv, O.R. Niyazova, Mechanisms of Formation and Migration of Defects in Semiconductors, Nayka, Moscow, 1981.
[23] V.A. Mukhanov, A.A. Kurakevich, V.L. Solozhenko, Interrelation of Hardness and Compressibility of Substances with Their Structure and Thermodynamic Properties, Superhard Materials, 6 (2008).